Dynamic Equivalent Modeling and Stability Analysis of Electric Power Systems

A Thesis Presented for the
Master of Science
Degree
The University of Tennessee, Knoxville

Xuemeng Zhang
August 2018

Copyright © 2018 by Xuemeng Zhang
All rights reserved.

ACKNOWLEDGEMENTS

First, I would like to express my deepest appreciation to my advisor, Dr. Yilu Liu, for her patient guidance and consistent encouragement in the past three years. In addition, I would also like to thank Dr. Fangxing Li, Dr. Husheng Li and Dr. Qing Cao as my dissertation committee members. I appreciate their precious time and valuable advice and comments on my paper.

Then, I would like to voice special thanks to those graduated Power IT Lab colleagues for their foundation work and contribution for my research, especially from Dr. Yong Liu, Dr. Shutang You, Dr. Ling Wu and Dr. Gefei Kou. My special gratitude is extended to all of my wonderful colleagues in FNET group: I am greatly appreciated the support and consistent friendship from Dr. Yu Su, Dr. Weikang Wang, Dr. Xiaotong Hu, Dr. Lin Zhu, Dr. He Yin and many other sincere friends. I also like to thank all my friends outside my academic life for the remarkable kindness and help. I will never forget the memorable time during the past three years in the University of Tennessee, Knoxville.

.

ABSTRACT

Interconnected power systems are increasing in both size and complexity. For such large-scale power systems, very accurate full-order dynamic system models are computational intensive to perform dynamic studies. In this paper, a measurement-based dynamic equivalent method is proposed to derive reduced models of large power systems. Specifically, a set of measurements at the boundary nodes between the study area and the external area are employed in model parameter identification. The proposed method is validated using simulation results obtained from both 140-bus NPCC system and 9,000-machine 70,000-bus U.S. Eastern Interconnection (EI) system. The results demonstrate that the measurement-based equivalent technique can capture the external system behaviors precisely. Compared with traditional generator equivalencing method, the proposed measurement-based model has higher accuracy but lower order and improved computational efficiency.

The intermittence and fluctuation of renewable generations bring unprecedentedly challenges to the power system reliability and resilience. To keep the lights on after contingencies such as the loss of two largest generation units, it is imperative for a power system to have sufficient frequency response reserve (FRR) to ensure that the decay in system frequency would be arrested before triggering under frequency load shedding (UFLS) schemes. In this paper, a method to derive the EI minimum FRR requirement in real-time will be developed. This minimum FRR will help the EI operators decrease the current FRR requirement and

accommodate more renewable generations while achieving a saving of both energy and facility costs. Most importantly, the ability to adaptively vary the FRR will provide the additional agility, resiliency, and reliability to the grid.

TABLE OF CONTENTS

Chapter One Mesurement-based Power System Dynamic Model Reductions 1
1.1 Introduction 1
1.2 Model Reduction Approach 4
1.2.1 Transfer Function Method 4
1.2.2 System Identification 5
1.2.3 Evaluation of the Model Accuracy 6
1.3 Case Study 8
1.3.1 Northeast Power Coordinating Council (NPCC) 8
1.3.2 Eastern Interconnection (EI) 12
1.4 Integrated Simulation in PSS/E 16
1.4.1 Results of 140-bus NPCC System 16
1.4.2 Results of 70,000-bus EI System 20
1.5 Conclusions 25
Chapter Two Real-time Minimum Frequency Response Reserve for Eastern Interconnection (EI) 26
2.1 Review of Frequency Response Concepts 29
2.1.1 Generation Trip Contingency 30
2.1.2 System Inertia 31
2.1.3 Governor Modeling 31
2.1.4 Load Frequency Sensitivity 33
2.1.5 Development of High Renewable Cases 34
2.2 Technical Approaches 36
2.2.1 Historical Inertia Values Analysis 36
2.2.2 Dispatch and Commitment Characterization 37
2.2.3 Minimum Frequency Response Reserve Determination 38
2.3 Conclusions 43
List of References 44
Vita 47

LIST OF TABLES

Table 1.1 Active power transfer functions 9
Table 1.2 Reactive power transfer functions 10
Table 1.3 Test contingencies 21
Table 2.1 First-stage UFLS of some power grids in the world 27
Table 2.1 Summary of Characteristics Metrics 38

LIST OF FIGURES

Figure 1.1 External and study areas of the power system. 5
Figure 1.2 Procedure of system identification 6
Figure 1.3 Approach of model reduction 7
Figure 1.4 NPCC one-line diagram 9
Figure 1.5 Measured and estimated results comparison 11
Figure 1.6 EI system map 13
Figure 1.7. FRCC geographical map 14
Figure 1.8 Comparison of different order transfer function 15
Figure 1.9 Integrated simulation results of the NPCC system 17
Figure 1.10 Integrated simulation results of the EI system 24
Figure 2.1 Frequency response of 1GW generation trip in EI and ERCOT 27
Figure 2.2 The EI system inertia change in a year 32
Figure 2.3 Frequency responsive modeling summary 33
Figure 2.4 Frequency responsive modeling for high renewable cases 35
Figure 2.5 frequency response of EI renewable cases 36
Figure 2.6 EI inertia value with 95 confidence intervals 37
Figure 2.7 Summary Metrics of various cases 39
Figure 2.8 Inertia value of various cases 39
Figure 2.9 EI frequency response to loss of 4.5GW generation 41
Figure 2.10 Real-time minimum FRR at UFLS 59.5Hz 42
Figure 2.11 Real-time minimum FRR at UFLS 59.3Hz 42

CHAPTER ONE MESUREMENT-BASED POWER SYSTEM DYNAMIC MODEL REDUCTIONS

1.1 Introduction

In today's interconnected power grids, it is difficult to analyze power system dynamics with a very accurate full-order dynamic system model, due to the increasing size, complexity, and nonlinearity of power systems. Thus, dynamic model reduction techniques are required to meet limited computational capabilities and accuracy requirements. In most cases, only a certain part of the system, called the internal or study area, is the primary focus of the study, while the rest can be reduced. Therefore, the main aim of providing system dynamic model reduction is to reproduce the aggregated steady-state and dynamic characteristics of the full-order network, while at the same time being compatible with the available computation tools for power system analysis.

Several dynamic reduction techniques have been developed in literature. In 1970's, Podmore [1] came up with the idea of coherency-based network reduction which became very popular and widely accepted, as it is able to give a physical picture of the reduced system. Recently, coherency-based methods have been extensively studied [2-4]. The basic idea is to identify coherent generators and replace them with a large equivalent and aggregated unit. Since the quality of the reduced model depends on the perturbation chosen for coherency identification and system operating conditions, the coherency has to be re-evaluated, thereby becoming time-consuming for large-scale interconnected power systems and

inappropriate for online analysis. Another model reduction approach, called modal method [5-6] simplifies the system by linear equations and preserves dominant modals. After eigenvalue analysis, generators in the external system that have no impact on the internal system are eliminated using controllability, observability and participation factors. However, this method requires detailed information of the system parameters which may not be accurate and cannot be updated in real time. Besides, balanced truncation method [7] and moment matching methods [8-9] have been successfully used in power system reduction. But the major bottleneck of balanced truncation-based approaches is their computational complexity.

Recently, some new methods have also been developed, such as measurement-based model reduction [10-13] and ANN-based boundary matching technique [14]. ANN (artificial neural network) technique is applied to the subject of dynamic equivalents due to its superior capability of capturing the dynamic characteristics of the external area. But it requires complicated neural network structures and substantial training data, which is hard to collect in practice. The measurement-based system identification method can utilize the real-time measurement from phasor measurement units (PMUs) and Frequency Disturbance Recorders (FDR) to reflect the actual system condition and to derive the dynamic faithful system model. The key issue is the parametrization of the target equivalent model without information on the configuration, parameters, or operating state of the external system.

Existing commercial software, e.g. EPRI's DYNRED program and DIgSILENT's PowerFactory software, largely rely on coherency-based methods. These dynamic reduction approaches are based on known circuit structure and parameters and can only be used for offline system analysis. Once the system dynamics change, the model has to be updated manually and will not be able to follow the system change fast enough in real time. For online dynamic security assessment, the knowledge of external system is usually unknown and then measurement-based methods offer advantages of authenticity and speed.

In our previous work [13], the autoregressive model (ARX) was employed to reduce external system. A PSS/E user-defined load-related model was developed to integrate the ARX model with the study system. Although the ARX model is accurate in predicting event response, it is tedious to develop user-defined model in PSS/E. Besides, only the zero-order ARX model has been studied which cannot represent the whole dynamic performance of the external system.

To meet both the model accuracy and time-critical requirements, this paper introduces a new equivalent model development method based on the transfer function, which directly utilizes the measured data such as the bus frequency, bus voltage, active and reactive power and identifies model parameters based on system identification techniques. The derived equivalents are integrated with a study system using a new user-defined model. Dynamic simulations are performed and corresponding results are evaluated.

1.2 Model Reduction Approach

A power system can be divided into the study area and the external area. The interface between the study area and the external area is defined by their n tie-lines and the corresponding buses shown in Figure 1.1.

In Figure 1.1, P_i and Q_i are the active and reactive power of the tie line i from external area to study area. V_i and f_i are the voltage magnitude and frequency of the buses.

For the external area, we will define the voltage magnitudes V_i and frequency f_i adjacent to interface as input signals, active power P_i and reactive power Q_i as output signals.

1.2.1 Transfer Function Method

Consider a linear time-invariant (LTI) system, for continuous-time input signal $u(t)$ and output $y(t)$, the transfer function is the linear mapping of the Laplace transform of the input, $U(s) = L\{u(t)\}$, to the Laplace transform of the output $Y(s) = L\{y(t)\}$:

$$G(s) = \frac{Y(s)}{U(s)}. \tag{1}$$

If the inputs and outputs of the system are determined, the system model can be represented as

$$\begin{bmatrix} y_1(s) \\ y_2(s) \\ \vdots \\ y_q(s) \end{bmatrix} = \begin{bmatrix} G_{11}(s) & \dots & G_{1p}(s) \\ G_{21}(s) & \dots & G_{2p}(s) \\ \vdots & \dots & \vdots \\ G_{q1}(s) & \dots & G_{qp}(s) \end{bmatrix} \begin{bmatrix} u_1(s) \\ u_2(s) \\ \vdots \\ u_p(s) \end{bmatrix}, \tag{2}$$

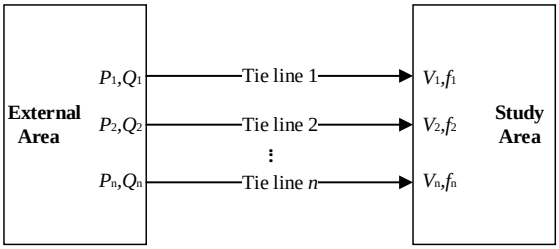


Figure 1.1 External and study areas of the power system.

where $G_{ij}(s)$ is the transfer function representing the relationship between input signal $u_j(s)$ and output signal $y_i(s)$.

1.2.2 System Identification

Generally, a transfer function can be used to determine important system response characteristics with selected inputs and outputs. The models only represent the mathematical relationship of the input signals and output data, which is not based on the physics of power system components described by differential-algebraic equations.

Two important features for the equivalent model are the order of the transfer function and the mathematical structure. To identify the transfer function of dynamic systems from measured input-output data, this paper uses the following steps as shown in Figure 1.2.

Step 1: Collect measurement data from the full-order system model. To estimate all model parameters, the dynamic response of the system (*P*, *Q*, *V*, *f*) is recorded for a disturbance.

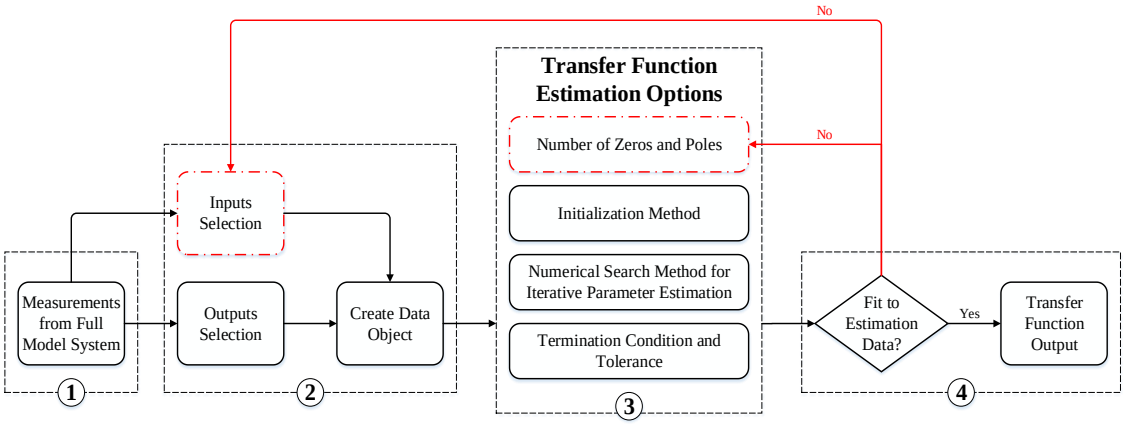


Figure 1.2 Procedure of system identification

Step 2: Define model inputs and outputs. Output signals are usually power flow of tie lines from external area to study area. Inputs can be any measurable signal in the study area.

Step 3: Train the model with selected inputs and outputs. Firstly, the number of zeros and poles should be defined. Initialization applies the instrument variable (IV) method. The numerical search uses the Gauss-Newton least squares method. The termination condition is set to 0.01 error, or 20 iterations.

Step 4: Output the model parameters for validation.

1.2.3 Evaluation of the Model Accuracy

The general idea of model accuracy evaluation is shown in Figure 1.3. Area 1 is the study area and Area 2 is the external area to be reduced. A tie line exists between Area 1 and Area 2. For example, the voltage and frequency of the border bus in the study area are used as inputs; active power and reactive power of the tie line are outputs. After training the transfer function with those inputs and

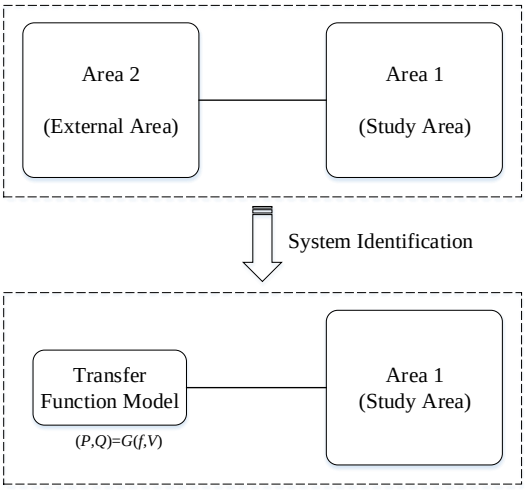


Figure 1.3 Approach of model reduction

outputs, a function $(P, Q) = G(f, V)$ in (2) can be obtained as the equivalent of the external system. The derived model is then used to predict results of the test events and its accuracy is evaluated by comparing its responses with that of the full model.

After identifying the transfer function model, it is necessary to validate whether the model is effective to represent dynamic response of the reduced area. The response of the identified model is compared with actual response.

$$MSE = \frac{1}{N}\sum_{k=1}^{N}\left(y(t_k) - y^{est}(t_k)\right)^2, \quad (3)$$

MSE is the Mean Squared Error between $y(t_k)$, the actual measured outputs, and $y^{est}(t_k)$, the simulated outputs, at time t_k. *N* is the number of sampling points. The smaller MSE is, the better the response of the reduced model matches actual response.

1.3 Case Study

To assess the effectiveness of proposed model reduction approach, two different study systems of different size are used in this paper.

1.3.1 Northeast Power Coordinating Council (NPCC)

This paper utilizes the Northeast Power Coordinating Council (NPCC) region system for the model accuracy test. The baseline model of the NPCC system used in this study is a reduced model with 140 buses and 48 machines. The total capacity of NPCC system is about 28 GW. Figure 1.4 shows its one-line diagram. In our study, the New England Power Pool (NEPOOL) is the external system to be reduced. As shown in Figure 1.4, the study area and external area are connected by two tie lines (blue solid lines: Bus#35 to Bus#73 and Bus#29 to Bus#37). A generation trip (red dot) at the study area (Bus#61) is used for model training. The inputs of the transfer function are voltage (V_1/V_2) and frequency (f_1/f_2) from the two buses (Bus#39 and Bus#38) near the interface. The outputs are active power (P_1/P_2) and reactive power (Q_1/Q_2) of two tie lines. Three different order transfer functions are estimated, whose accuracy is compared with the original model shown in Table 1.1 and Table 1.2. Measured active power (P_1) and simulated active power in zero-order, first-order and second-order transfer functions are plotted in Figure 1.5(a). Figure 1.5(b) shows the measured and estimated reactive power (Q_1).

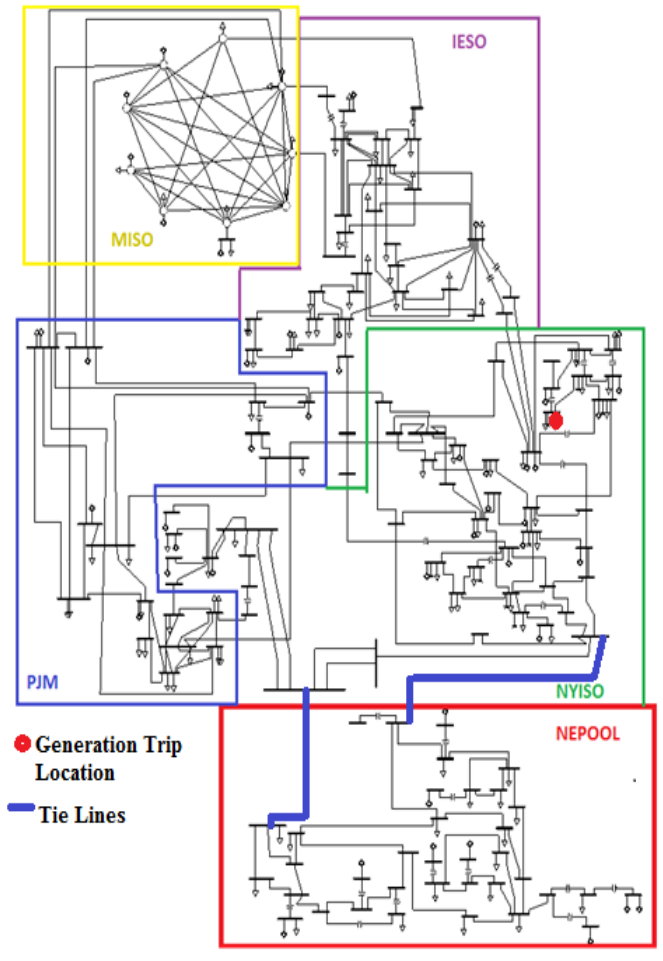


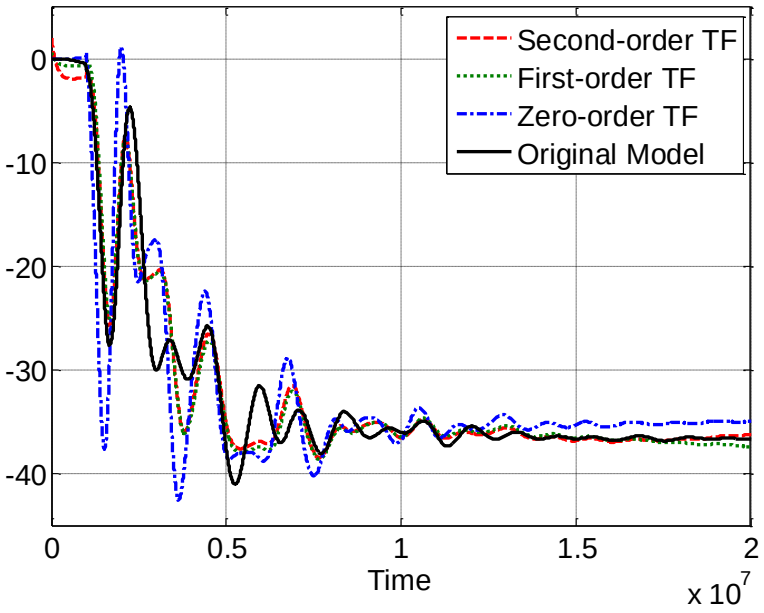
Figure 1.4 NPCC one-line diagram

Table 1.1 Active power transfer functions

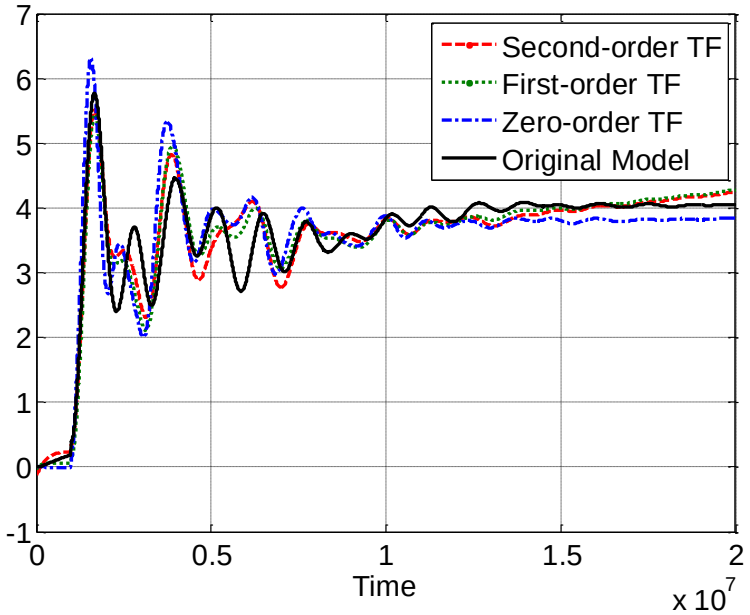
Orders	Active Power Transfer Function	Accuracy
zero	$231100f + 4548V$	57.14%
First	$\frac{-1.659 \times 10^4 s + 1.241}{s + 6.781 \times 10^{-6}} f + \frac{3907s - 0.001442}{s + 6.378 \times 10^{-8}} V$	76.98%
Second	$\frac{-1.873 \times 10^4 s^2 + 1.246s - 1.68 \times 10^{-7}}{s^2 + 6.698 \times 10^{-6} s + 3.29 \times 10^{-13}} f + \frac{3831s^2 - 0.002035s - 1.093 \times 10^{-9}}{s^2 + 4.137 \times 10^{-8} s + 1.054 \times 10^{-14}} V$	77.61%

Table 1.2 Reactive power transfer functions

Orders	Reactive Power Transfer Function	Accuracy
zero	$-2.14 \times 10^4 f + 720.3V$	53.94%
First	$\frac{-809.1s - 0.1185}{s + 8.171 \times 10^{-6}} f + \frac{883.5s + 0.0002156}{s + 3.313 \times 10^{-8}} V$	70.29%
Second	$\frac{-6586s^2 - 0.05938s - 2.788 \times 10^{-8}}{s^2 + 1.089 \times 10^{-6} s + 1.717 \times 10^{-12}} f + \frac{1044s^2 - 0.0005034s + 8.997 \times 10^{-10}}{s^2 + 4.717 \times 10^{-6} s + 9.62 \times 10^{-14}} V$	68.4%



(a) Active power



(b) Reactive power

Figure 1.5 Measured and estimated results comparison

The result shows that the first-order and second-order models demonstrate higher accuracy than the zero-order model. The first-order and second-order transfer function effectively capture dynamic response of the full power system, while the response of the zero-order function has relatively large deviations from that of the original model. Usually, original dynamic models in the external area are high-dimensional. The zero-order function has lower accuracy because it reduces original full order system onto a very low-dimensional subspace, which cannot represent the whole dynamic performance of the external area.

1.3.2 Eastern Interconnection (EI)

To demonstrate the effectiveness of the proposed approach, a case study was performed on the Eastern Interconnection (EI) system. The baseline model of the EI system used in this study is a detailed dynamic model with 70,000 buses and 9,000 machines. The total generation capacity of this model is about 590 GW. Figure 1.6 shows its geographical map with major transmission lines reflected.

In our study, the Florida Reliability Coordinating Council (FRCC) is the study system, as shown in Figure 1.7, which is connected to SERC Reliability Corporation by two tie lines (denoted in yellow solid lines: Bus No. 1 to Bus No. 3 and Bus No. 2 to Bus No. 3). Besides FRCC, the rest of the EI system, which has 66,000 buses and 8,300 machines, is reduced using proposed transfer function model.

A generation trip (red dot) at the study area (Bus No. 4) is used for model training. The inputs of the transfer function are voltage (V) and frequency (f) from the border

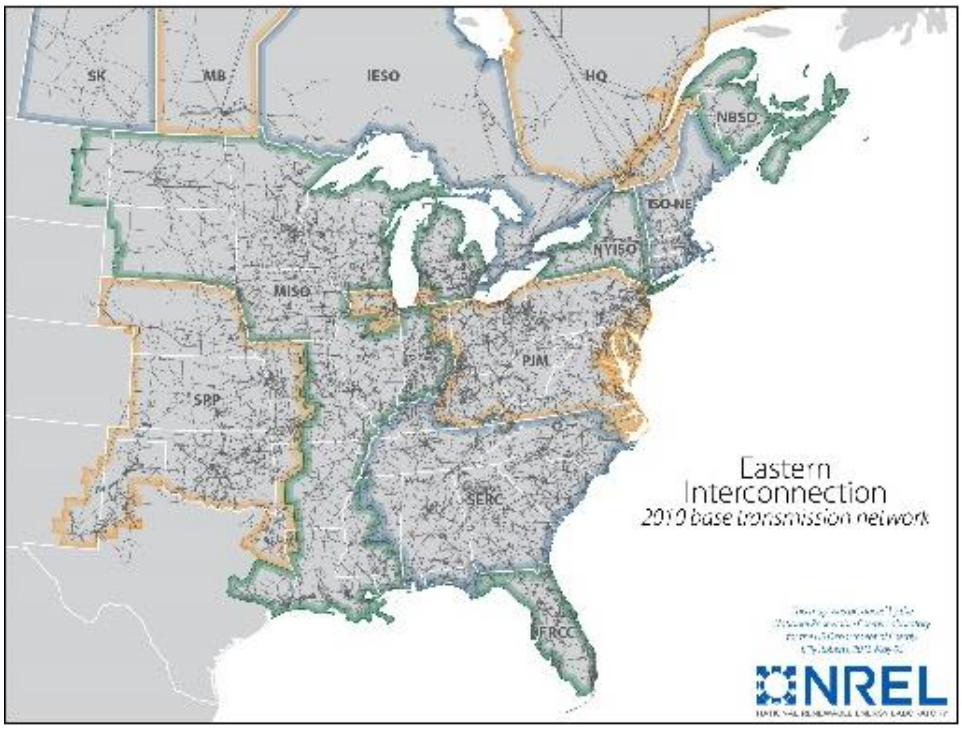


Figure 1.6. EI system map

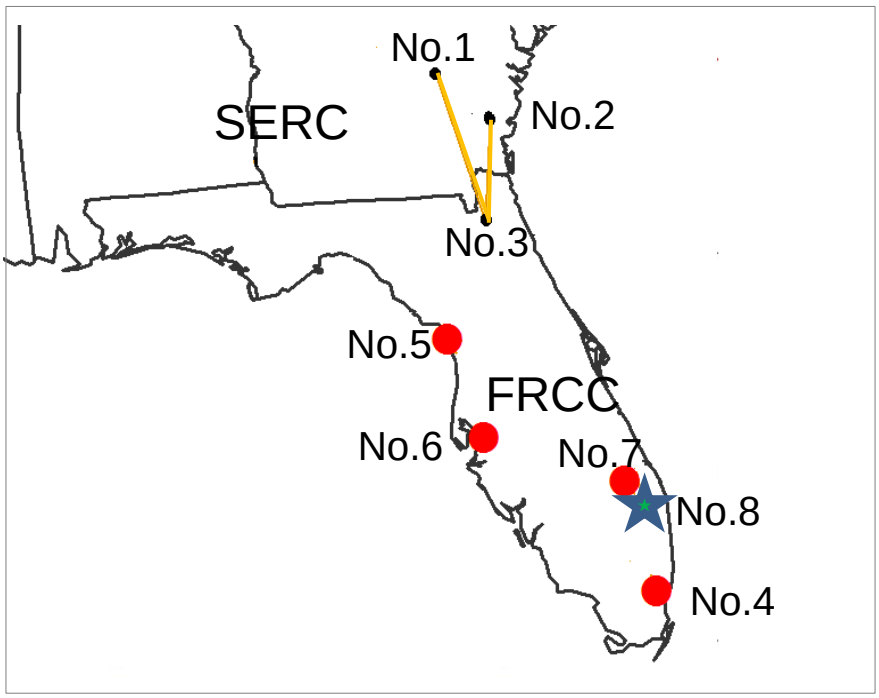


Figure 1.7. FRCC geographical map

bus (Bus No. 3) of tie lines. The outputs are active power (P_1/P_2) and reactive power (Q_1/Q_2) of two tie lines. Theoretically, more measurement signals would improve model accuracy but, unfavorably, increase complexity. To reduce model complexity, input signals with low correlation with output signals can be omitted. In this paper, since the transfer function represent dynamic response of power flow at tie lines, frequency and voltage are selected as inputs since they are typical inputs of controllers, such as governors and exciters.

Another important feature of a transfer function is its order. Generally, a higher order is more complex but may not demonstrate higher accuracy. A comparison of transfer functions with different orders is shown in Figure 1.8.

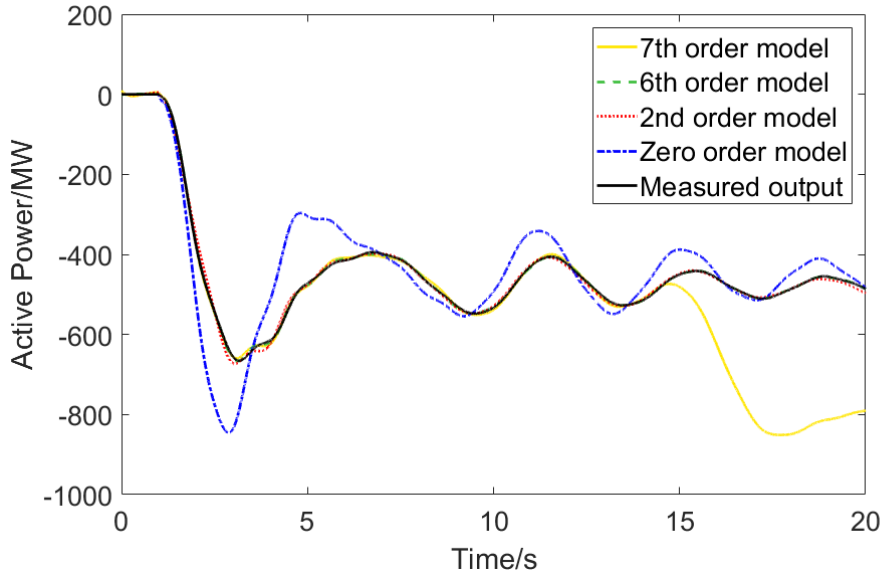


Figure 1.8 Comparison of different order transfer function

The results show that a higher order model generally has higher accuracy. However, there is no significant improvement in accuracy when the model order increases from second to sixth. The seventh order model even results in over fitting. In this study case, the second-order model is adequate in accuracy and thus considered the appropriate reduced model of the external system. For general applications, the optimal number of model orders depends on system characteristics, accuracy requirements, computation resources, and the model implementation constraint in simulation environments (for example, high-order user-defined models are difficult to incorporate in PSS/E).

1.4 Integrated Simulation in PSS/E

Since PSS/E can accomplish nonlinear time domain simulations for the large-scale power system efficiently, this paper attempts to construct the equivalent model for the NPCC system and EI system under PSS/E with the procedure directly implemented in it. The equivalents are developed in both load flow model and dynamic model.

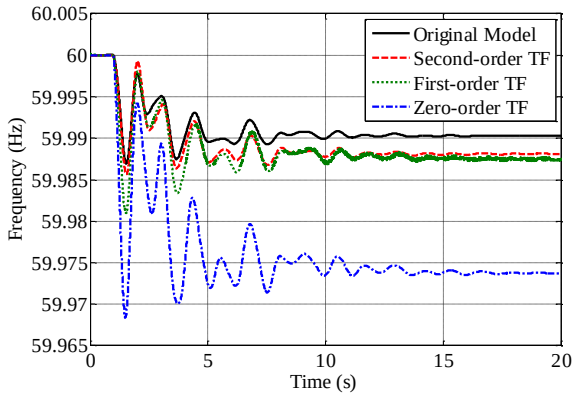
1.4.1 Results of 140-bus NPCC System

In order to implement the transfer function in power system analysis software PSS/E, a user-defined generic network element (GNE) model provided by GMB software is applied to control active and reactive power outputs according to the reduced model. Inputs of GNE are frequency f and voltage V.

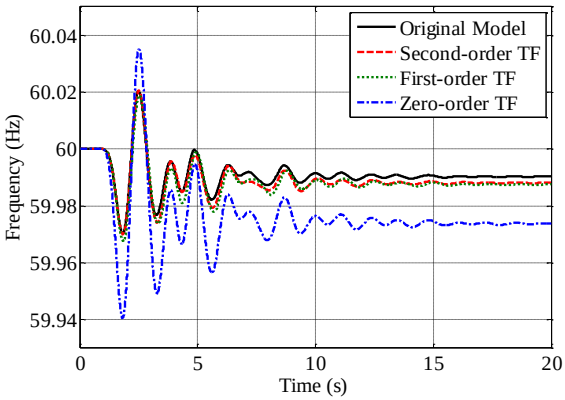
Using the procedure in Figure 1.2, each tie line between the study area and the external area is replaced by connecting the GNE element to the border bus in the study area. The disturbance is a generation trip in the study area and three different transfer functions in Table 1.1 and Table 1.2 are implemented. The results of the reduced model and full model are compared. Frequency, voltage, active power and reactive power at the study area and interface location are shown in Figure 1.9.

Results show that frequency of the higher order transfer function is closer to the response of the original model, both at the interface and the study area. Second-order transfer function successfully captures swings compared with the original

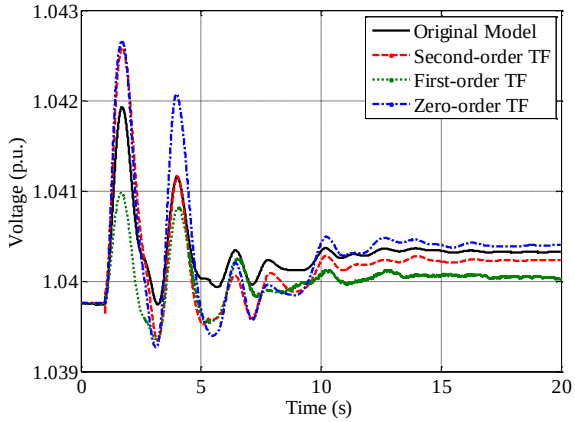
Figure 1.9 Integrated simulation results of the NPCC system



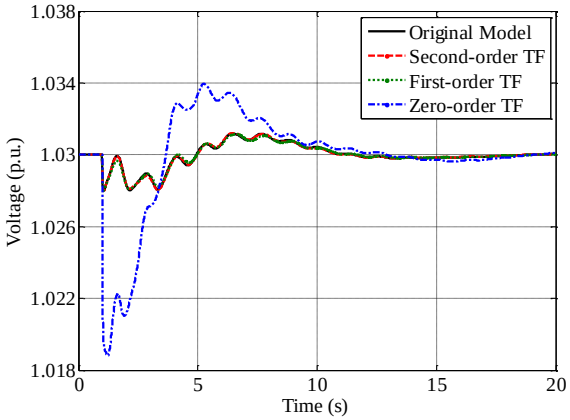
(a) Frequency (interface 1)



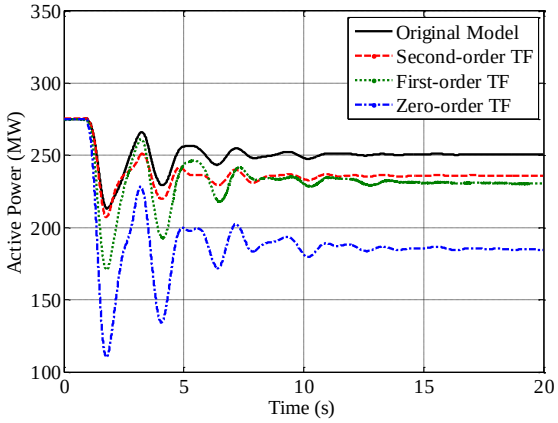
(b) Frequency (study area)



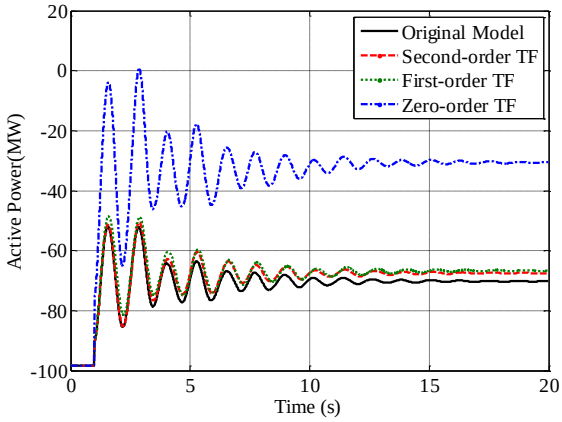
(c) Voltage (interface 1)



(d) Voltage (study area)

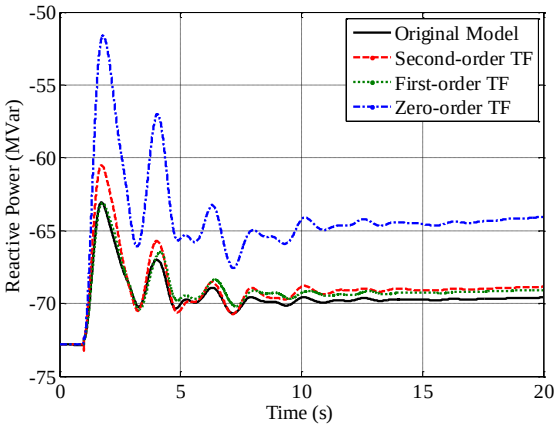


(e) Active Power (interface 1)

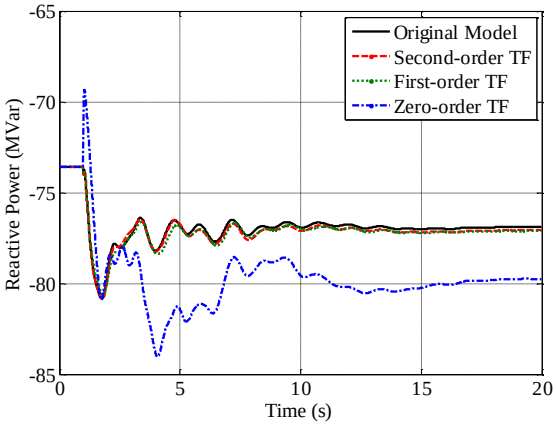


(f) Active Power (study area)

Figure 1.9 continued



(g)Reactive Power (interface 1)



(h) Reactive Power (study area)

Figure 1.9 continued

model, while their settling frequency is not consistent due to that the accuracy of those three models is not 100%.

The voltage at interface does not match perfectly in those three different models as shown in Figure 1.9(c). However, in Figure 1.9(d), the voltage in the study area using first-order and second-order transfer function matches very well with the original model. It is noticed that in Table II, the first-order reactive power transfer function has higher accuracy than second-order, which is verified by the reactive power profiles shown in Figure 1.9(g).

1.4.2 Results of 70,000-bus EI System

In order to implement the transfer function in power system analysis software, a user-defined model is written in FORTRAN and integrated in PSS/E to control active and reactive power outputs according to the trained model.

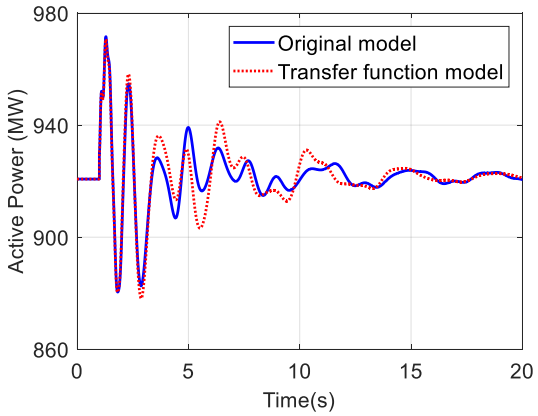
Using the procedure in Figure 1.2, the influence of each tie line (between the study area and the external area) on the study area is represented by a user-defined model connected to the border bus in the study area (Bus No. 3). To validate the performance of the transfer function model, four different generation trips as listed in Table 1.3 are applied. Active power and reactive power at the observation location (indicated by the green star in Figure 1.7) following four contingencies are shown in Figure 1.10. The similarity between responses of the reduced model and those of the original model shows that transfer function can effectively capture the behavior of the full system.

Table 1.3 Test contingencies

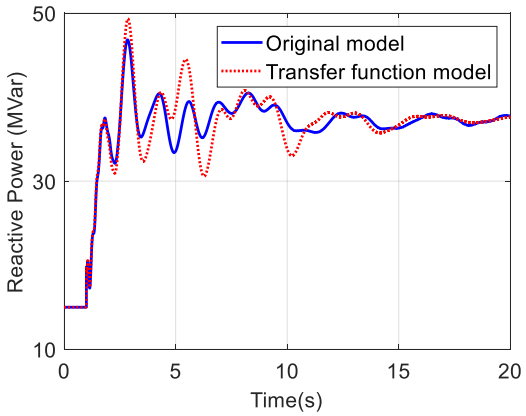
Contingency	Generation Trip Bus	Trip Amount (MW)	*MSE*	
			P	*Q*
Con_1	4	1237	19.4812	3.0804
Con_2	5	1078	3.2192	0.5184
Con_3	6	1078	11.7651	1.3455
Con_4	7	1078	4.7960	0.3777

Table 1.3 also listed the MSE values, indicating that the measurement-based equivalent model has relatively high accuracy in representing the external system. With the external system reduced, to the measurement-based model, the complexity scale of the new model is around 5% of that of the full-order system model, substantially increasing the simulation speed.

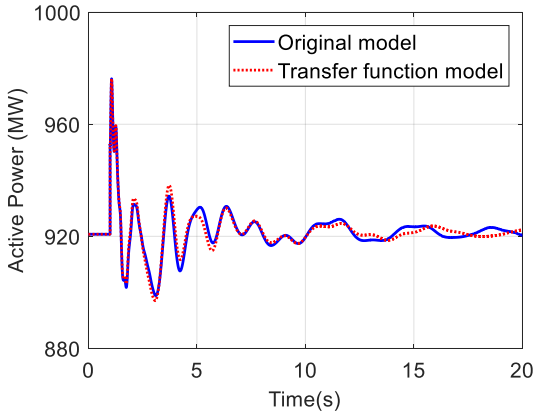
Figure 1.10 Integrated simulation results of the EI system



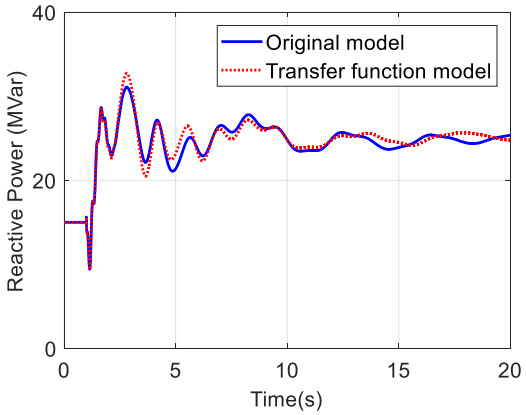
(a) Active power (Con_1)



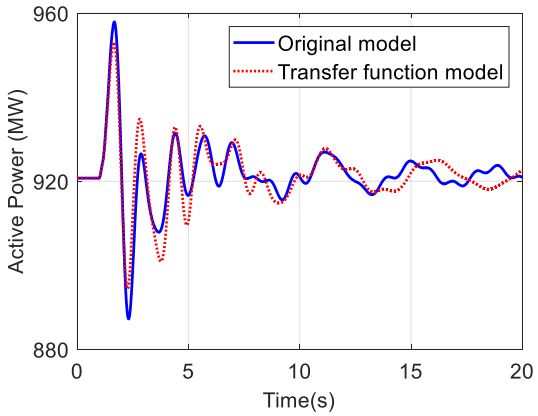
(b) Reactive power (Con_1)



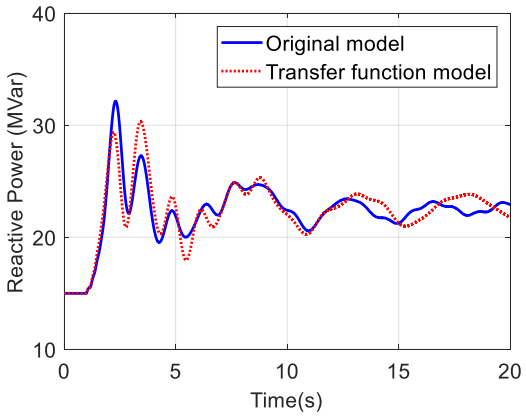
(c) Active Power (Con_2)



(d) Reactive power (Con_2)

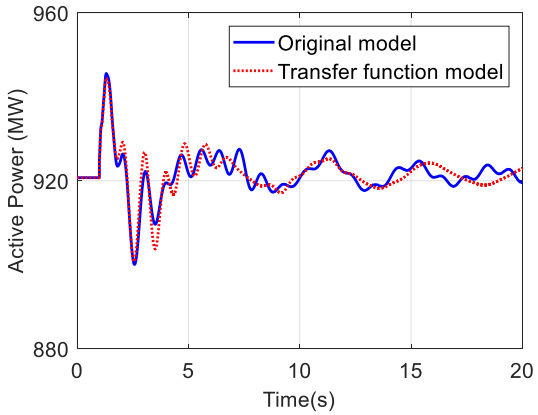


(e) Active power (Con_3)

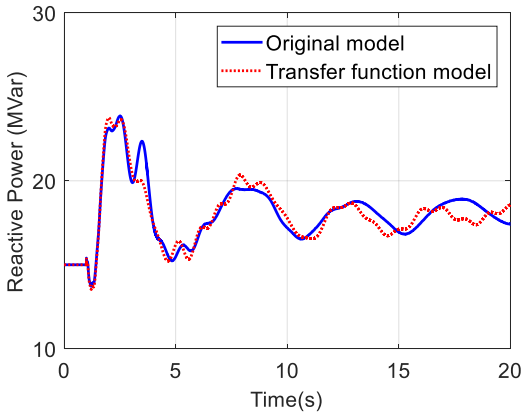


(f) Reactive power (Con_3)

Figure 1.10 Continued



(g) Active power (Con_4)



(h) Reactive power (Con_4)

Figure 1.10 Continued

1.5 Conclusions

Measurement-based system reduction can overcome the disadvantages of traditional model-based techniques and it is more suitable for online update with the increasing availability and quality of wide-area measurement data. In this paper, a measurement-based transfer function model is proposed for model reduction and multiple tie lines between the study area and the external area can be replaced by the reduced model. Transfer functions with different orders are compared and the model accuracy is tested on the NPCC system and EI system. A PSS/E user-defined model is developed to integrate the reduced model to the study area. Results show that the transfer function is accurate in presenting the dynamics of the external system.

CHAPTER TWO REAL-TIME MINIMUM FREQUENCY RESPONSE RESERVE FOR EASTERN INTERCONNECTION (EI)

The intermittence and fluctuation of renewable generations bring unprecedentedly challenges to the power system reliability and resilience. To keep the lights on after contingencies such as the loss of two largest generation units, it is imperative for a power system to have sufficient frequency response reserve (FRR) to ensure that the decay in system frequency would be arrested before triggering under frequency load shedding (UFLS) schemes. However, maintaining an adequate FRR involves significant consumption of energy and the consequent production costs for the interconnection.

Historically, the Eastern Interconnection (EI)'s FRR has been maintained at a level much higher than necessary. Several major ISOs and electric utilities such as Dominion Energy, ISO-NE, and PJM have voiced such concerns. As shown in Figure 2.1, the EI's frequency nadir is much higher than that of the ERCOT after a 1 GW generation loss contingency. Furthermore, the UFLS in EI allows much smaller frequency excursions than most power grids in the world (as shown in Table 2.1). Australia and several other countries are considering further relaxing their UFLS thresholds for renewable integration and it will be merely uneconomical to maintain a very tight frequency requirement based on the worst scenario.

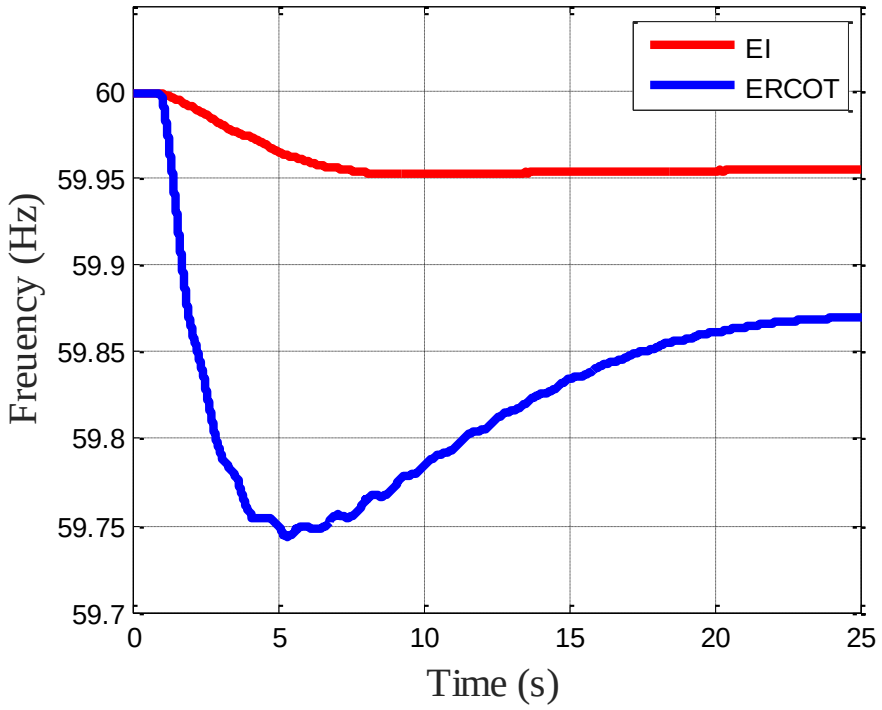


Figure 2.1 Frequency response of 1GW generation trip in EI and ERCOT

Table 2.1 First-stage UFLS of some power grids in the world

Power Grid	**Nominal Frequency**	**First-stage UFLS threshold**
EI, US	60	59.5
ERCOT, US	60	59.3
Australian Energy Market Operator	50	49
National Grid, UK	50	48.8
Transpower, New Zealand	50	47.8

As noted in the LBNL 2010 Study [15], the FRR of the EI was sufficient to maintain reliability with the increases in variable renewable generation projected at that time. The findings in that study pointed out two aspects of primary frequency control: First, the characteristic "lazy L" shape of frequency response in the EI (see Figure 2.1). Unlike the other North American systems (ERCOT), the frequency nadir in the EI is not lower than the settling frequency. This “Lazy-L” response is also reflected in the $\mathrm{CB_R}$ metric, which is “the statistically determined ratio of Point C to Value B” (NERC BAL-003-1). In other North American systems, $\mathrm{CB_R}$ is greater than 1.0, meaning that the nadir is at a lower frequency than the settling frequency. The EI settling frequency is lower on average than the initial nadir, so $\mathrm{CB_R}$ is limited to 1.0. Consequently, the IFRO (-1,002 MW/0.1 Hz) is proportionately smaller to the design-basis event in the EI compared to the other interconnections.

LBNL 2010 study concluded that “Lazy L” is driven by withdrawal of primary frequency response by plant load controllers. Study discussed the detrimental effect of withdrawal on interconnection frequency response, and investigated a major reason for withdrawal, which is the setting on plant load controllers. As observed, an appropriate setting can prevent withdrawal during frequency response event. Thus, it is significantly important that industry engineers and planners implement reliable and stable operating policies that prevent detrimental withdrawal of primary frequency response.

Secondly, the recognition of withdrawal of primary frequency response encourages planners to improve the quality of the interconnection’s dynamic

planning models to replicate and explain the interconnection's observed frequency response. IFRO of EI is established by the largest event in the last 10 years, however the Eastern Interconnection planning models currently developed and used by industry do not reproduce the performance of the interconnection that was recorded during that generation-loss event. Well-calibrated planning models are essential for assessing current performance, ensuring continued, reliable interconnection frequency response. Many efforts have been taken to continuous updating and ongoing calibration of the planning models to study future scenarios involving increases in the renewable generation.

2.1 Review of Frequency Response Concepts

System frequency experiences an immediate decline due to loss of a large amount of generation, which is referred to frequency response. Consider the frequency response metrics, rate of change of frequency (ROCOF) is determined by the amount of rotating mass (mechanical inertia) in the interconnection; the combination of inertia and Primary Frequency Response (PFR) dictates frequency nadir; after the frequency decline has been arrested, continued delivery of PFR will stabilize frequency at a steady-state settling level. Therefore, the proper modeling of mechanical inertia and governor has significant impact on the accurate representation of interconnection frequency response. If the loss of generation is large enough and generators do not respond rapidly and arrest the decline in frequency, power system frequency may decline below established, safe operating bounds and trigger automatic, emergency load shedding to avoid a cascading

blackout. To ensure reliable frequency response at all times, advance planning and corrective actions are required, because generation-loss events are always unpredictable and frequently occurring issues.

The characteristics of interconnection frequency largely depends on four physical factors:

1. The size of the generation-loss event;
2. The interconnection's inertia, which determines the rate of change of frequency (ROCOF);
3. Primary frequency control from turbine governors, which respond immediately to changes in frequency and power; and
4. Secondary and tertiary frequency control, the former is implemented by plant-level controllers; the latter takes centrally coordinated actions to re-dispatch generation.

In this paper we consider the actions of primary control, while the power plant secondary control, grid-level balancing and tertiary controls are not our study of interest.

2.1.1 Generation Trip Contingency

For EI, the largest event in the last ten years is the loss of 4,500MW of generation, indicated in NERC BAL-003-1 Standard (August 4, 2007) [16]. That's the design basis event for the NERC Interconnection frequency response obligation (IFRO). Standard also identifies 59.5Hz as the 'first step' of under-frequency load shedding (UFLS), which is intended to be a safety net to prevent against system collapse

from severe contingencies. The goal is to avoid triggering the first step of UFLS following resource contingency criterion.

2.1.2 System Inertia

Since the purpose of FRR is to keep the frequency nadir above the UFLS threshold after a major contingency, the system inertia at the time of contingency should be taken into consideration in determining the minimum FRR. This is because frequency nadir is significantly influenced by system inertia. Furthermore, as shown in Figure 2.2, the observed total system inertia of EI varies a lot over time (June 2016 to July 2017). With the increasing renewable generation, the inertia variation will be even more dramatic. However, the inertia information historically has not been given enough weight in determining the EI system's existing FRR requirement, leading to an overly conservative FRR value requirement.

To represent system inertia in our model, generators are classified as two types: generators that contribute inertia and generators that do not contribute inertia. Variable renewable generation (like wind turbines and solar photovoltaic generator) does not contribute inertia to the power system. For those generators that contribute inertia, they can be divided according to whether they do or do not response to frequency deviations (i.e., provide PFR).

2.1.3 Governor Modeling

As discussed, the sole means by which interconnections ensure reliable operation following the sudden unplanned loss of a generator is through primary frequency

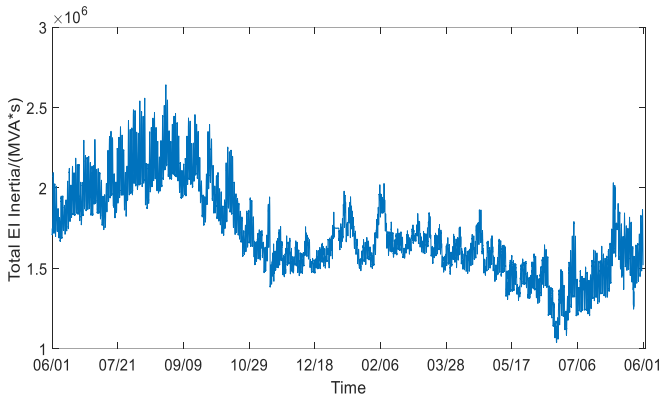


Figure 2.2 The EI system inertia change in a year

response delivered by generation (or equivalent resources such as demand or storage) with headroom. Several key factors could affect delivery of primary frequency response: (1) the faction of generators that respond to changes in frequency; (2) the headroom from which response can be provided by these generators; (3) the rate at which technology-specific turbine-governors deliver PFR from this headroom. To simplify it, we divide generators that contribute inertia into two categories: those that do and those that do not participate in primary frequency control. The portion that participates in primary frequency control is the frequency responsive generation and the portion that does not participate is the non-frequency responsive. To illustrate key relationships and interactions among the factors that influence interconnection frequency response, we collected information on the portion of units equipped with and without governors (see Figure 2.3).

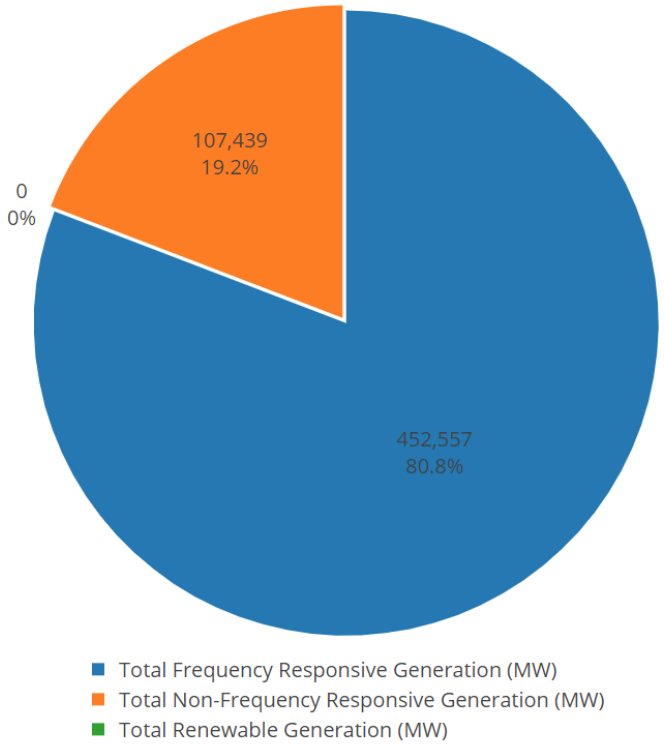


Figure 2.3 Frequency responsive modeling summary

For the on-line generation, 19.2 percent of the dispatched generators are modeled without governors and are therefore non-frequency responsive. The remaining percent of the on-line dispatched generators are frequency responsive.

2.1.4 Load Frequency Sensitivity

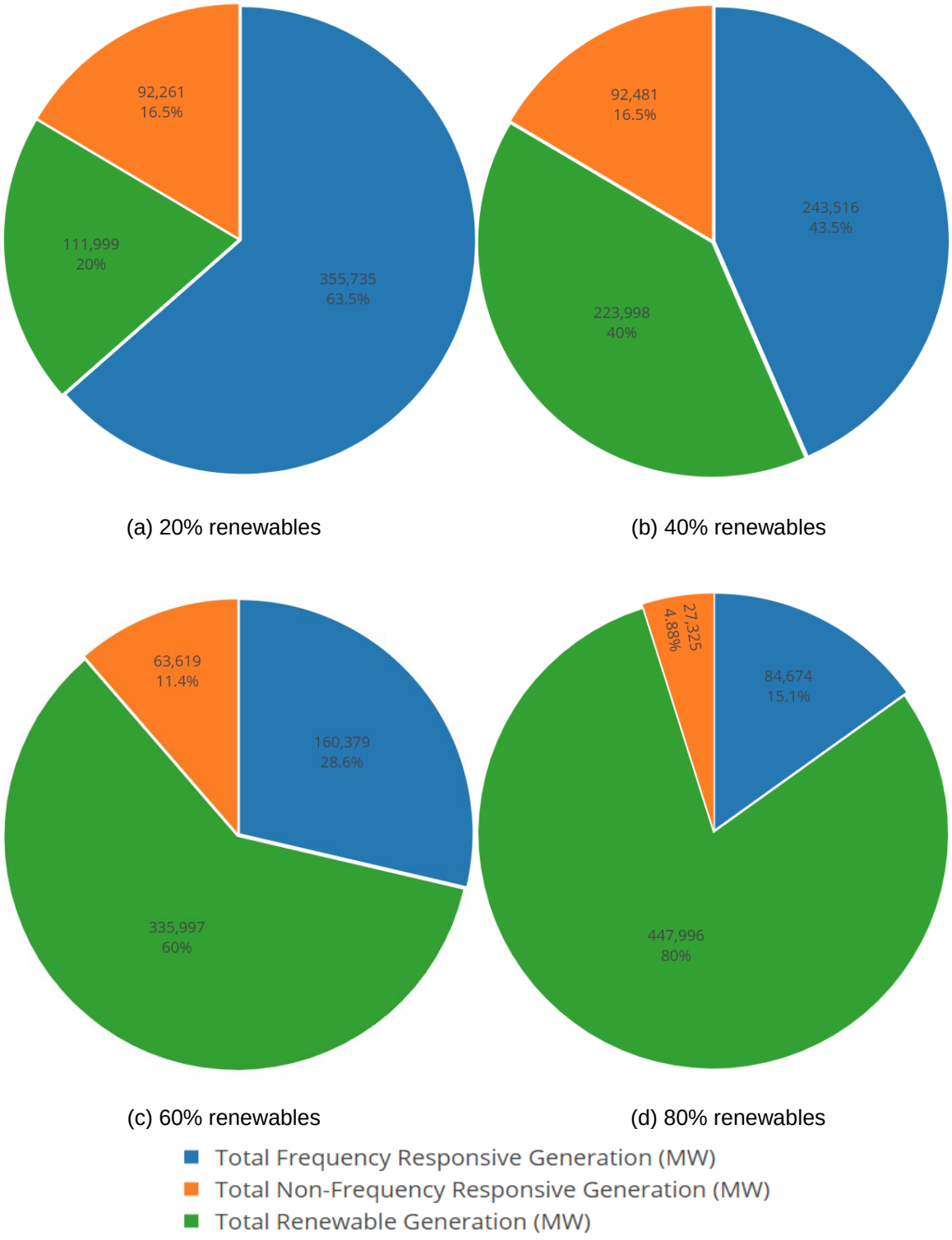
Some portion of load responds to changes in interconnection frequency. Historically, load damping or load sensitivity supported the delivery of primary frequency response from generators [17]. In rotor speed equation, D represents the variation of *electrical load* with frequency, as seen from the generator. The parameter, D, gives an *approximate* representation of the damping effect

contributed by the speed sensitivity of system loads. The value of D could range from near zero for systems with predominantly resistive load to approximately two for systems with a large percentage of pumping, fan, and other industrial load.

Since a portion of load has traditionally reduced consumption autonomously in proportion to a decline in interconnection frequency and therefore augments primary frequency control by generators, it is stipulated that the total system load decreases as frequency decreases. Meanwhile, It is clear that the frequency sensitivity of the load contributes measurably to both the initial arrest of frequency decline and the subsequent recovery.

2.1.5 Development of High Renewable Cases

To study the effect of changes in system inertia on the requirements for primary frequency control, we vary the percent of generation that contributes inertia. To build new cases to verify FRR requirement under different inertia conditions, the level of renewable (wind and solar PV) generation by replacing a portion of conventional generators with PV and wind plants. The total renewable penetration rate is chosen to be 20%, 40%, 60% and 80% as shown in Figure 2.4. These four levels of renewable penetration should be able to largely reflect EI renewable integration in the following several decades. Their frequency response after 4.5GW generation trip disturbance is shown in Figure 2.5. As shown, EI system has adequate frequency response reserve for all these five frequency curves are above UFLS threshold (59.5 Hz), even in 80% renewable case. If all governors are tuned



(a) 20% renewables

(b) 40% renewables

(c) 60% renewables

(d) 80% renewables

Figure 2.4 Frequency responsive modeling for high renewable cases

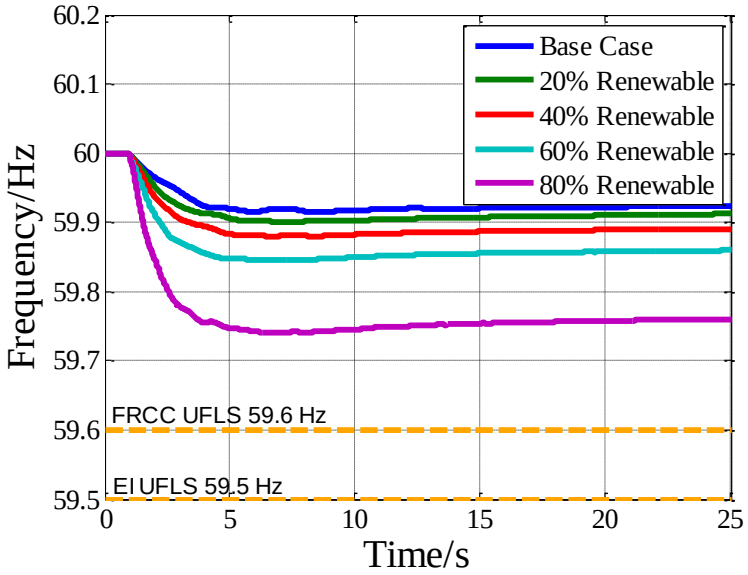


Figure 2.5 frequency response of EI renewable cases

on in the renewable cases, frequency response can be significantly improved. To further decay frequency drop, we pick a sequence of governors to be removed.

2.2 Technical Approaches

2.2.1 Historical Inertia Values Analysis

In this task, the historical inertia value of the EI system (already provided by NERC) is analyzed statistically. The hourly, daily, monthly, and even yearly patterns of EI inertia value is investigated and the probability distribution of these inertia values is obtained. Based on these analyses, a set of representative inertia values is selected for later FRR study. The general guideline for the representative inertia selection is more inertia values should be selected in the inertia range with a higher probability density. In Figure 2.6, 0.95 confidence level is selected for determining

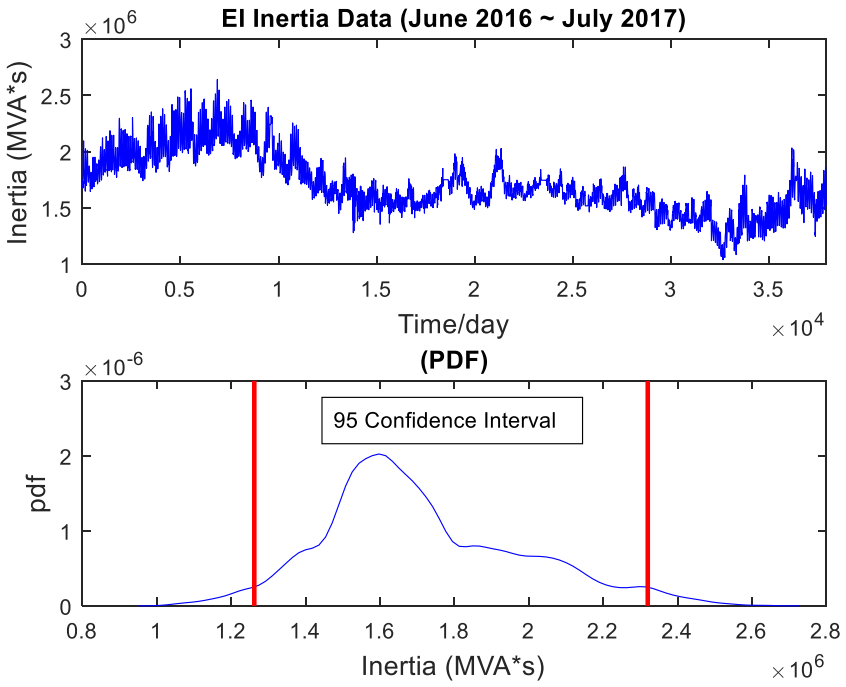


Figure 2.6 EI inertia value with 95 confidence intervals

the probability that the confidence interval produced will contain the true inertia value. The presentative inertia range is from $1.26e^6$ to $2.32e^6$ MVA*s.

2.2.2 Dispatch and Commitment Characterization

The FR of the system is dominated by the amount and type of generation committed and how it is dispatched. According to the power flow and dynamic data, each of generators in the study system can be characterized as GR units that have governor models and will provide FR, NG units will not provide FR and renewables (wind and PV). Table 2.1 summarize important aspects of the initial conditions used for various cases, where

GR Pgen (GW): Power generation of units with GR,

Table 2.1 Summary of Characteristics Metrics

Metrics	base	20%	40%	60%	80%
GR Pgen (GW)	452.6	355.7	243.5	160.4	84.7
GR MWCAP (GW)	609.3	496.9	372.2	274.2	119.5
GR Headroom (GW)	156.7	141.2	128.7	113.8	34.8
GR MVA (1000 MWA)	637.8	509.6	364.6	247.5	125.7
Inertia (MVA*s)	$1.93e^6$	$1.61e^6$	$1.22e^6$	$7.71e^5$	$3.86e^5$

GR MWCAP (GW): Power generation (MW) capability of units with GR,

GR Headroom (GW): Headroom of units with GR,

GR MVA (1,000 MVA): MVA of units with GR,

Inertia (MVA*s): Total inertia value of system.

Figure 2.7 compares the critical characteristics of the generation that relate to frequency performance of various cases. Generation that provides GR running on the system is used to quantify overall system readiness to provide FR. Figure 2.8 shows inertia conditions of those cases.

2.2.3 Minimum Frequency Response Reserve Determination

As mentioned earlier, system inertia will influence the frequency nadir after a generation trip contingency, thus the minimum FRR must be calculated independently for each given inertia value. In this task, the minimum FRR will be determined through dynamic simulations at each of the inertia levels selected from Section 2.1. Specifically, after tuning the EI model's inertia to a representative

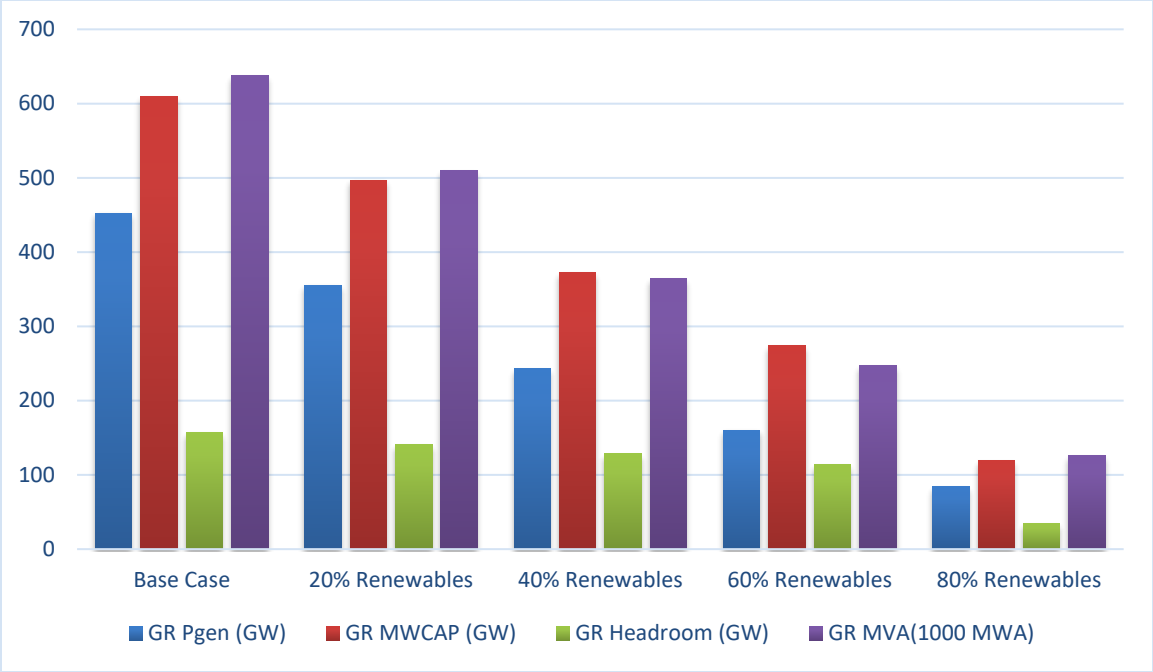


Figure 2.7 Summary Metrics of various cases

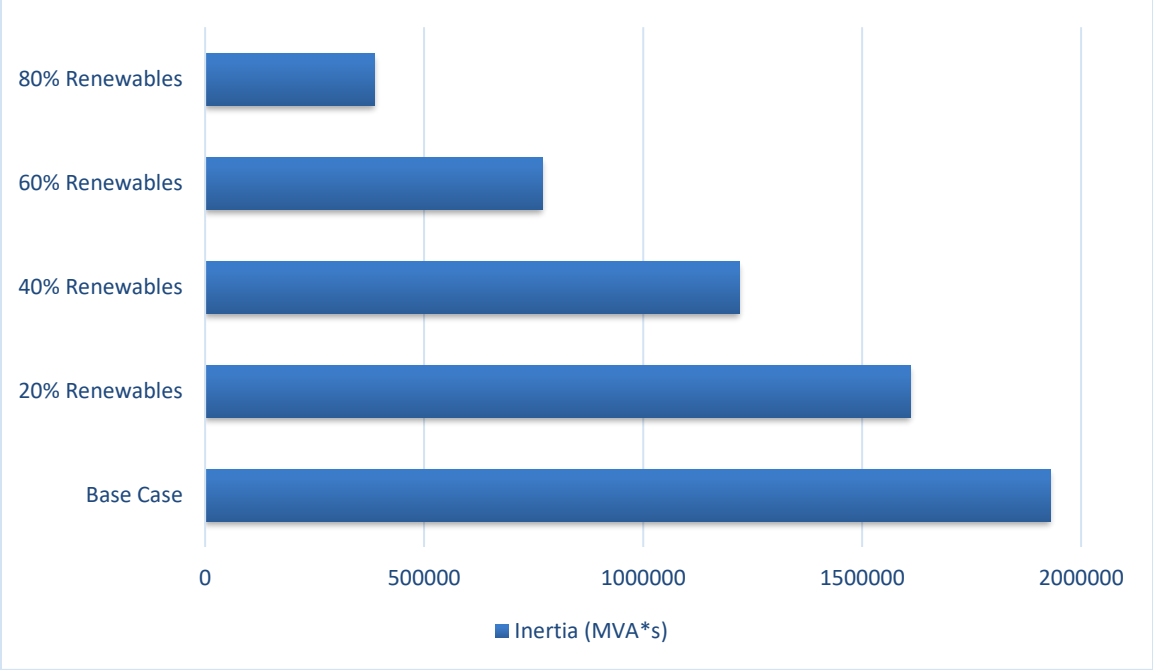


Figure 2.8 Inertia value of various cases

inertia value, the FRR of the EI model will be decreased gradually in order to make frequency nadir fall to the UFLS threshold. This FRR value will be the threshold minimum FRR at this inertia level (see Figure 2.9). Current EI UFLS settings and resource contingency criteria (4.5 GW generation loss) is used in this task.

In Figure 2.9, at a given inertia value, system frequency nadir and settling value are determined by governor response, which is usually quantified by ‘headroom’. When system governor response decreases, frequency curve has lower nadir and settling frequency value. In such case, dark red curve with 9060.1MW headroom is defined as minimum frequency response reserve.

As mentioned, headroom indicates the difference between the current operating point of a generator or transmission system and its maximum operating capability. The headroom available at a generator establishes the maximum amount of power that generator theoretically could deliver to oppose a decline in frequency.

However, “headroom” is not the only contribution of responsive fraction of each interconnection’s generation fleet. Many required information includes how the output of each generator is controlled and how each generator is dispatched also influence FRR calculation. For example, a generator may be capable in principle of participating in primary frequency control, but if it is dispatched at its maximum operating point (e.g., a baseload generating plant or a wind generating plant), it does not have headroom available from which primary frequency response could be delivered. Similarly, a generator operating with headroom whose turbine-

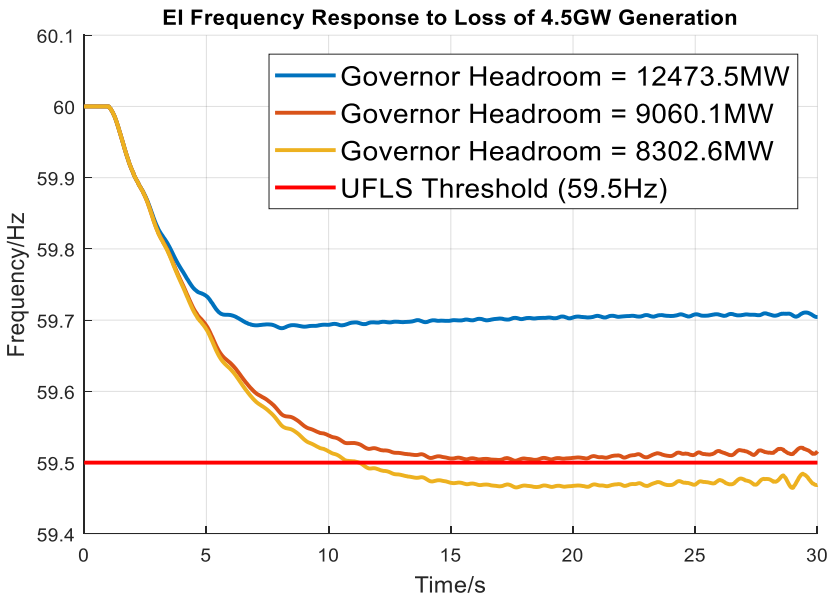


Figure 2.9 EI frequency response to loss of 4.5GW generation

governor controls are blocked or operated with a very large deadband (e.g., > 300 mHz) will not participate in primary frequency control.

In our EI study system, most generators with governor response has overestimated headroom value, which means the calculated headroom value is not accurate in representing FRR. To better represent FRR, we use GR MVA in this study. Figure 2.10 shows a negative relationship between FRR and inertia at given 59.3Hz UFLS threshold.

As mentioned, EI has more stringent UFLS requirements than other North American interconnections. For example, the first stage UFLS threshold in EI is 59.5 Hz, comparing to 59.3 Hz in ERCOT. If the EI first-stage UFLS setpoint can be decreased to 59.3 Hz, the minimum FRR requirement for EI can be further

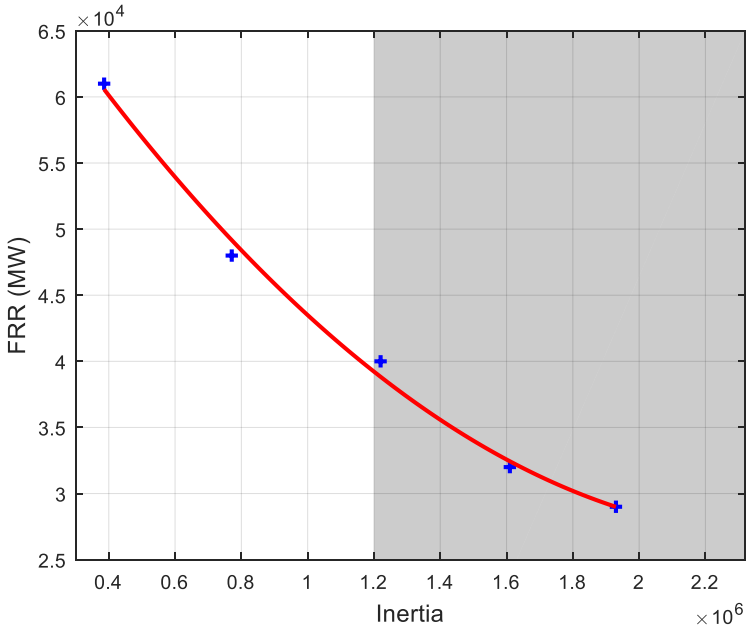


Figure 2.10 Real-time minimum FRR at UFLS 59.5Hz

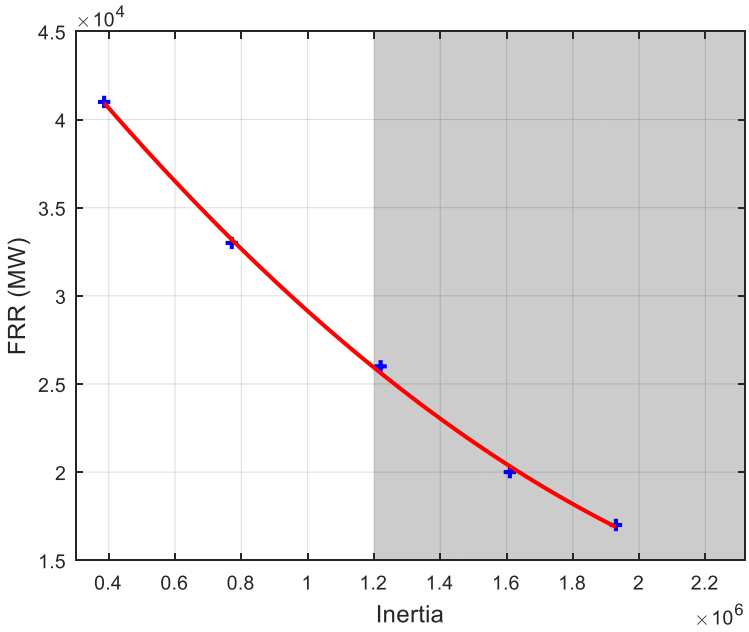


Figure 2.11 Real-time minimum FRR at UFLS 59.3Hz

decreased, saving even more energy and production cost for the EI utilities and electricity consumers (see Figure 2.11).

2.3 Conclusions

This project mainly focused on frequency response assessment, including the impact of the proposed Ancillary Services: synchronous inertial response and primary frequency response. Detailed dynamic simulations were performed in this assessment to evaluate the system frequency response in the first 20~30 seconds following a frequency event. A criteria to determine the minimum PFR is to calculate GR MVA when frequency nadir >= 59.5 Hz with the loss of 4.5GW generation. Study showed when system with a high penetration of renewable integration, more FRR is required to maintain secure and reliable operating condition.

LIST OF REFERENCES

[1] Podmore, Robin. "Identification of coherent generators for dynamic equivalents." *IEEE Transactions on Power Apparatus and Systems* (1978): 1344-1354.

[2] Nath, Ram, Surrinder S. Lamba, and KS Prakasa Rao. "Coherency based system decomposition into study and external areas using weak coupling." *IEEE Transactions on Power Apparatus and Systems* (1985): 1443-1449.

[3] Chow, Joe H., et al. "Inertial and slow coherency aggregation algorithms for power system dynamic model reduction." *IEEE Transactions on Power Systems* (1995): 680-685.

[4] Joo, Sung-Kwan, et al. "Coherency and aggregation techniques incorporating rotor and voltage dynamics." *IEEE Transactions on power systems* (2004): 1068-1075.

[5] Verghese, G. C., I. J. Perez-Arriaga, and F. C. Schweppe. "Selective modal analysis with applications to electric power systems, Part II: The dynamic stability problem." *IEEE Transactions on Power Apparatus and Systems* (1982): 3126-3134.

[6] de Oliveira, Sebastiao EM, and J. F. De Queiroz. "Modal dynamic equivalent for electric power systems. I. Theory." *IEEE Transactions on Power Systems* (1988): 1723-1730.

[7] Safonov, Michael G., and R. Y. Chiang. "A Schur method for balanced-truncation model reduction." *IEEE Transactions on Automatic Control* (1989): 729-733.

[8] Celik, Mustafa, and Andreas C. Cangellaris. "Simulation of multiconductor transmission lines using Krylov subspace order-reduction techniques." *IEEE Transactions on Computer-Aided Design of Integrated Circuits and Systems* (1997): 485-496.

[9] Chaniotis, Dimitrios, and M. A. Pai. "Model reduction in power systems using Krylov subspace methods." *IEEE Transactions on Power Systems* (2005): 888-894.

[10] Chakrabortty, Aranya, Joe H. Chow, and Armando Salazar. "A measurement-based framework for dynamic equivalencing of large power systems using wide-area phasor measurements." *IEEE Transactions on Smart Grid* (2011): 68-81.

[11] Wang, Shaobu, et al. "Dynamic-feature extraction, attribution, and reconstruction (DEAR) method for power system model reduction." *IEEE transactions on power systems* (2014): 2049-2059.

[12] Hesen Liu, Lin Zhu, Zhuohong Pan, Feifei Bai, Yong Liu, Yilu Liu, Mahendra Patel, Evangelos Farantatos, Navin Bhatt. “ARMAX-based Transfer Function Model Identification Using Wide-area Measurement for Adaptive and Coordinated Damping Control”, *IEEE Trans. Smart Grid* (SCI), 2015, to appear.

[13] Chai, Jidong, et al. "Measurement-based system reduction using autoregressive model." *Transmission and Distribution Conference and Exposition (T&D), 2016 IEEE/PES*. IEEE, 2016.

[14] F. Ma and V. Vittal, "A Hybrid Dynamic Equivalent Using ANN-Based Boundary Matching Technique," *IEEE Trans. Power Syst.*, vol. 27, no. 3, pp. 1494-1502, Aug. 2012.

[15] Undrill, J.M. (2010). *Power and Frequency Control as it Relates to Wind-Powered Generation*. Lawrence Berkeley Laboratory. LBNL-4143E. December 2010.

[16] NERC. (2015d). *Standard BAL-003-1.1—Frequency Response and Frequency Bias Setting.* Effective April 1, 2005, as amended though November 13, 2015.

[17] Eto, J., J. Undrill, P. Mackin, R. Daschmans, B. Williams, B. Haney, R. Hunt, J. Ellis, H. Illian, C. Martinez, M. O'Malley, K. Coughlin, and K. Hamachi-LaCommare. (2010). *Use of a Frequency Response Metric to Assess the Planning and Operating Requirements for Reliable Integration of Variable Renewable Generation.* LBNL-4142E. Berkeley: Lawrence Berkeley National Laboratory. December.

[18] NERC (2017b). *2017 Frequency Response Annual Analysis*. NERC. November.

VITA

Xuemeng Zhang received the B.S. degree from Zhejiang University in 2015. She is currently working towards her M.S. degree in electrical engineering at the University of Tennessee, Knoxville. Her research interests include power system dynamic analysis and renewable energy integration.